Solution Structure of a Double Mutant of the Carboxy-Terminal Dimerization Domain of the HIV-1 Capsid Protein[†,‡]

Hing C. Wong,[§] Ronald Shin,[§] and N. Rama Krishna*[,§,||]

Comprehensive Cancer Center and the Department of Biochemistry & Molecular Genetics, The University of Alabama at Birmingham, Birmingham, Alabama 35294-2041

Received November 5, 2007; Revised Manuscript Received December 17, 2007

ABSTRACT: As in other retroviruses, the HIV-1 capsid (CA) protein is composed of two domains, the N-terminal domain (NTD) and the C-terminal domain (CTD), joined by a flexible linker. The dimerization of the CTD is thought to be a critical step in the assembly of the immature and mature viral capsids. The precise nature of the functional form of CTD dimerization interface has been a subject of considerable interest. Previously, the CTD dimer was thought to involve a face-to-face dimerization observed in the early crystallographic studies. Recently, the crystallographic structure for a domain-swapped CTD dimer has been determined. This dimer, with an entirely different interface that includes the major homology region (MHR) has been suggested as the functional form during the Gag assembly. The structure determination of the monomeric wt CTD of HIV-1 has not been possible because of the monomer−dimer equilibrium in solution. We report the NMR structure of the [W184A/M185A]-CTD mutant in its monomeric form. These mutations interfere with dimerization without abrogating the assembly activity of Gag and CA. The NMR structure shows some important differences compared to the CTD structure in the face-to-face dimer. Notably, the helix-2 is much shorter, and the kink seen in the crystal structure of the wt CTD in the face-to-face dimer is absent. These NMR studies suggest that dimerization-induced conformational changes may be present in the two crystal structures of the CTD dimers and also suggest a mechanism that can simultaneously accommodate both of the distinctly different dimer models playing functional roles during the Gag assembly of the immature capsids.

The assembly of the cone-shaped mature capsid of the human immunodeficiency virus type 1 (HIV-1[1]) is the culminating point of a sequence of events that starts with the multimerization of the 55 kDa Gag polyprotein at the plasma membrane of the infected cell, release of the spherical immature virus particle composed of radially arranged Gag proteins, viral budding, cleavage of the Gag by viral protease that releases its major subunits MA, CA, and NC, and finally the condensation of the CA proteins to form a conical capsid that encapsulates NC, the RNA, and other viral enzymes (*1*−*3*). The detailed structures of many of the proteins involved at various stages in the above sequence of events have been investigated by crystallography and NMR spectroscopy and recently reviewed (*4*).

The 231-residue long HIV-1 capsid protein (CA) consists of two apparently independently folding domains, viz., the N-terminal domain (NTD) and the C-terminal domain (CTD), joined by a flexible linker. Its inherent flexibility, the tendency to oligomerize, and its monomer−dimer equilibrium have frustrated attempts at the structure determination of the full-length CA. The structure of the wt NTD monomer has been reported (*5*). A similar structure determination of the monomeric form of wt CTD has not been possible because of the monomer−dimer equilibrium, and current structural knowledge is based on the crystal structures of the isolated CTD dimers (*6*−*8*). Considerable mutational data exist, identifying specific functional residues in the full-length CA required for assembly and infectivity (*9*−*11*). In *in vitro* assembly reactions, the CA protein forms long helical tubes as well as cones that resemble mature capsids (*12*−*15*). According to the recently prevailing model supported by image reconstruction analyses of electron cryo-micrographs (*16*) and molecular docking of the NTD and CTD structures, the HIV-1 capsid surface appears to be composed of hexameric rings of NTD domains joined to neighboring hexameric rings through the interring CTD dimerization. Thus the CTD domain plays a critical role as the dimerization domain during assembly (*3*).

The wt CA from HIV-1 exhibits a monomer−dimer equilibrium in solution with a K_d of ∼18 μM, and most of the dimeric interface is located in the CTD domain (*6*). Two distinctly different models for the CTD:CTD dimeric inter-

[†] The NMR measurements were performed at the NMR Core Facility of the Cancer Center supported by NCI Grant 1P30 CA-13148.

[‡] The structural constraints together with the coordinate files for the family of 30 structures (PDB ID 2jyg) and the energy-minimized average structure (PDB ID 2jyl) have been deposited with the RCSB Protein Data Bank.

* Corresponding author: N. Rama Krishna, Department of Biochemistry & Molecular Genetics, CH19-B31, 1530-3rd Ave South, University of Alabama at Birmingham, Birmingham, AL 35294-2041. Phone: (205) 934-5695. Fax: (205) 934-6475. E-mail: nrk@uab.edu.

[§] Comprehensive Cancer Center.

[||] Department of Biochemistry & Molecular Genetics.

[1] Abbreviations: HIV-1, human immunodeficiency virus type 1; CA, capsid protein; CTD, carboxy-terminal domain of CA; MHR, major homology region.

10.1021/bi7022128 CCC: $40.75
Published on Web 01/26/2008

face have been proposed based on crystallographic studies. In the face-to-face dimer (*6*, *7*), the dimer interface is composed of parallel packing of helix-2 (residues 179−192) from each monomer creating a hydrophobic core involving residues Val181, Trp184, Met185, and Leu189. The residues in the 3_{10} helix are also involved in the dimeric interface (*7*). The available mutational data are generally compatible with the notion that the face-to-face dimeric interface may play a critical role in capsid assembly and HIV-1 replication: (i) W184A and M185A mutations significantly weaken dimeric association in solution. This is compatible with the observation that CA proteins with these mutations assemble significantly slower than the wt CA in concentration (*17*). (ii) Capsid (CA) assembly reactions with either of these mutations abrogate infectivity and lead to assembly defects (*10*). (iii) The interface residues W184 and M185 appear to be required for high fidelity assembly since Gag assembly reactions with a W184A and/or M185A CA leads to the formation of irregular shaped virus-like particles (*9*, *10*, *18*). However, arguments against the significance of a face-to-face dimer include the following (*8*): (i) most of the retroviral CA proteins exist as monomers in solution (*19*−*21*), (ii) the residues at the face-to-face dimeric interface are not conserved, and finally (iii) this interface does not readily explain the remarkable conservation of major homology region (MHR) among the retroviral capsid proteins.

Most recently, Ivanov et al., (*8*) reported the crystal structure of a domain-swapped dimer of Δ177-CTD mutant which resembles the face-to-face dimer except that helix-1 from each of the monomers swap positions, thereby creating a distinctly different dimeric interface for the CTD dimer. The HIV-1 CTD is a structural homologue of the mammalian SCAN dimer which was shown to exhibit a domain-swapped dimer structure (*22*). Most importantly, the dimeric interface in the HIV-1 CTD now involves the MHR region, thereby providing an explanation for the remarkable conservation of this region among the retroviral capsid proteins and for the mutational data on the MHR region. They proposed that the kink or deviation from ideal geometry seen in helix-2 in the monomers of other retroviral CA proteins as well as a similar kink presumed to exist in the monomeric HIV1 CTD may provide the driving force for the formation of the domain-swapped dimer during Gag assembly. Interestingly, residues W184 and M185 appear to be involved only in a peripheral manner in the dimeric interface of the domain-swapped dimer, thereby suggesting that their mutations may not have as pronounced an effect on the dimeric interface. It may well be that the domain-swapped dimeric interface model may be restricted to Gag assembly as originally envisioned by Ivanov et al. (*8*).

We note that while the HIV-1 CA protein readily forms dimers in solution presumably through a face-to-face dimerization (and it is the only retroviral CA known so far that has high enough affinity to form dimers with reasonable concentrations in solution), and the two separate crystal structures of isolated CTD dimers give valuable insights on plausible models on the dimerization interface, it is only the presence of such dimeric interfaces under the *in vivo* and *in vitro* assembly conditions for Gag and CA assembly that are relevant.

In this work we report the NMR structure of the W184A/M185A CTD in its monomeric form. Though this structure shows overall similarity to the wt CTD structure in the face-to-face dimer, there are some significant differences: (1) the helix-2 is significantly shorter in the double mutant CTD compared to the wt CTD. (2) Helix-4 is slightly longer in the NMR structure. (3) The well-defined kink seen in helix-2 in the wt CTD crystal structure is absent, and (4) the loop between helices 1 and 2 is longer in the double mutant CTD. On the basis of our results, we suggest that the crystal structures of the CTD dimers may contain dimerization-induced conformational changes. We also discuss below the implications of our findings on Gag and CA assembly.

While this manuscript was in preparation, the NMR structure of W184A-CTD from HIV-1 CA has just been published (*23*). The NMR structure of the single mutant differs significantly (rmsd ∼ 12 Å) from our NMR structure of the double mutant. We suggest some possible explanations for these differences.

MATERIALS AND METHODS

Cloning, Protein Purification, and Characterization. Plasmid for the expression of the W184A/M185A mutant CTD was obtained from Prof. Peter Prevelige, Jr., at UAB. The vector used for expressing the W184A/M185A mutant CTD was pET15b, which carried a His(6X) tag and a thrombin cleavage site. The vector was transformed into *E. coli* BL21-(DE3). Individual bacterial colonies were placed into 10 mL starter culture tubes containing 5 mL of LB medium and 100 μg/mL ampicillin. The starter cultures were grown overnight at 37 °C and then added to flasks containing M9 minimal media (*24*). Labeling was accomplished by using uniformly labeled ^{15}N ammonium chloride and/or ^{13}C glucose as the nitrogen and/or carbon sources, where needed. The flasks were shaken at 200 rpm in a thermally controlled agitator/incubator, and the cultures were grown until the optical density at 600 nm was approximately 0.8. The cells were induced using 1 mM IPTG and were harvested by centrifugation (6000*g* for 10 min). Lysis was accomplished using 60 s of sonication bursts in a buffer containing 50 mM phosphate (pH 5.0), 3 mM sodium azide, 10 mM DTT, and 1 mM EDTA. The lysates were centrifuged at 20000*g* for 30 min, and the cell pellets were discarded. The protein of interest was separated using incremental ammonium sulfate precipitation, and the pellets from the 75% ammonium sulfate fraction were retained. The pellets were dialyzed against the above buffer several times and loaded onto a Q-Sepharose column containing a similar buffer. The flowthrough was collected and analyzed for protein content using reducing SDS-PAGE. Pure fractions were collected and concentrated using centrifugal concentrators. After concentration, the protein solutions were buffer exchanged with the identical buffer but using deuterated compounds where appropriate. The protein with the intact His-tag was used for NMR measurements. The NMR sample conditions were ∼1 mM protein, 50 mM sodium phosphate, pH 5, with 3 mM sodium azide, 5−10 mM deuterated DTT, 1 mM deuterated EDTA, 0.1 mM AEBSF, and 1/100 of the protease inhibitor cocktail tablet (from Roche).

Multidimensional NMR Spectroscopy. All the 3D-NMR experiments were done at 30 °C on a Bruker Avance 600 NMR spectrometer equipped with a TXI probe. The following 3D-NMR measurements were performed on the doubly

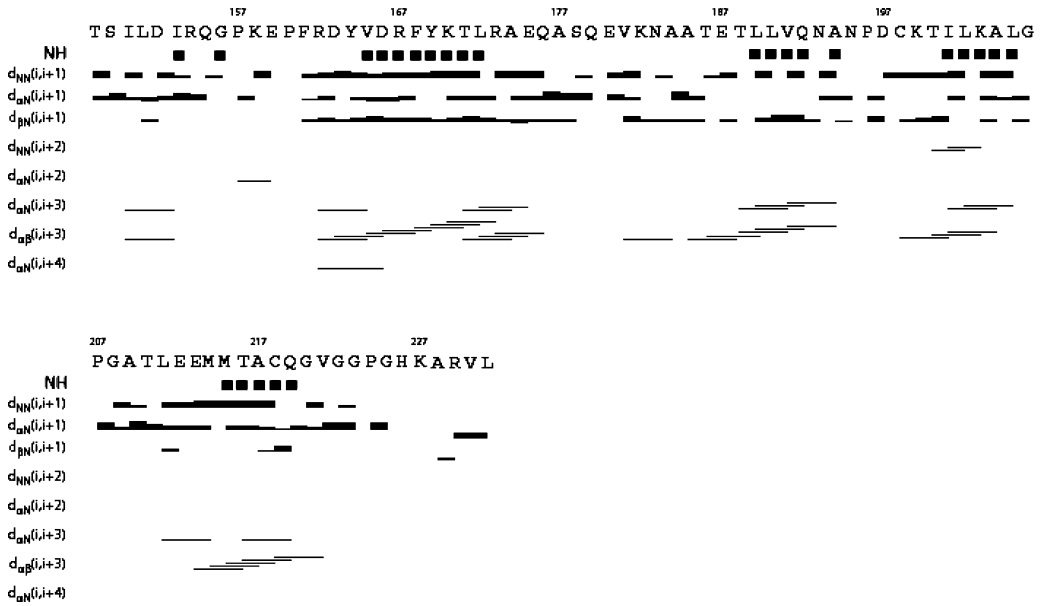

FIGURE 1: Sequential connectivities observed in the W184A/M185A-CTD mutant together with a summary of slowly exchanging amide protons (NH). The thickness of the bars qualitatively represents the intensities of the NOE connectivities.

labeled CTD sample: HNCA (80 × 44 × 1024), HNCACB (120 × 48 × 1024), HNCO (96 × 60 × 1024), CBCACONH (120 × 48 × 1024), HCCH−TOCSY (128 × 64 × 2048), and HCCH−COSY (128 × 64 × 2048). In addition, HNHA (44 × 128 × 2048), ^{15}N-HSQC-NOESY (144 × 40 × 2048, mixing time of 150 ms) and ^{13}C-HSQC-NOESY (200 × 90 × 2048, mixing time of 150 ms) were also performed. The NMR data were processed using a sine bell window function with 60° shift in all dimensions, zero filled, without linear prediction using NMRPipe (*25*), and analyzed with XEASY (*26*).

The amide hydrogen H/D exchange experiment was performed by dissolving freeze-dried protein in 100% D_2O at pH 4 and recording the ^{15}N-HSQC spectrum. The total elapsed time from dissolving the protein in D_2O to the finish of the NMR run was about 50 min. Thus the only amide protons that persisted in the HSQC spectrum are those with half-lives of 25 min and longer and are identified as exchange-protected amide protons in structure refinement calculations. Solvated amide protons (excepting for the amide proton next to the C-terminal carboxylate group) typically have exchange life times varying from 0.1 to 200 s at pH 4 and 30 °C depending upon the inductive effects (*27*−29) of the side chains on either side and will not be detected in the HSQC spectrum.

Structure Refinement Calculations. Structure calculations were performed with the software program CYANA. The His-tag was not included in the structure calculations. Structures were initially calculated using only NOE distance restraints. Restraints that caused large violations were subjected to reexamination and reassignment. Dihedral angle restraints, which were obtained from HNHA experiment and the program TALOS, were added in the calculation. Hydrogen bond distance restraints were introduced on the basis of the results of the H/D exchange experiments for only those amide hydrogens where an acceptor CO group was readily identifiable on the basis of the prefinal structures. All of the acceptor CO groups were in the backbone except for 156 NH and 195 NH which appeared close to the side chain CO groups of 159 and 155 respectively in the prefinal structures, and so these hydrogen bonds were included in the final refinement. Inclusion of these two hydrogen bonds did not affect the structures. In the final calculation, 500 structures were calculated, and 30 structures with the lowest target functions were selected. The average of these structures was calculated and energy minimized using the "minimize" command in CYANA using default values. The first minimization was done with the presence of the constraint file. Then, the constraint file was removed and the structure was subjected to about 100 cycles of energy minimization until no further reduction was seen in the target function. Next, this structure was further energy minimized using the GROMOS force field (*30*) with default parameters in Swiss PDB-Viewer to generate the final energy-minimized average structure.

RESULTS

Figure 1 shows the experimentally determined sequential NOE connectivities observed in the double mutant CTD together with a summary of slowly exchanging amide protons. The NMR assignments were made using one-bond and two-bond heteronuclear correlations observed in a suite of 3D-NMR experiments. A representative family of 30 structures of the W184A/M185A-CTD generated by CYANA calculations is shown in Figure 2 while a ribbon model of the energy-minimized average structure is shown in Figure 3 together with a model for the wt CTD in the face-to-face dimer for comparison (*6*, *7*). The structural statistics for the NMR structures are given in Table 1. The secondary structure elements include a short 3_{10} helix involving residues 150−152, and four helices involving residues 161−174 (helix-1), 186−193 (helix-2), 196−205 (helix-3), and 211−220 (helix-4). Residues 222−231 at the carboxy terminus are disordered. The Supporting Information contains a figure of the energy-minimized average NMR structure of the double mutant with all the side chains. Figure 4 shows the best-fit superposition of residues within the four helices between our energy-minimized average NMR structure and the wt CTD

FIGURE 2: A family of 30 structures of W184A/M185A-CTD from CYANA calculations. The secondary structural elements (see text) are shown in purple.

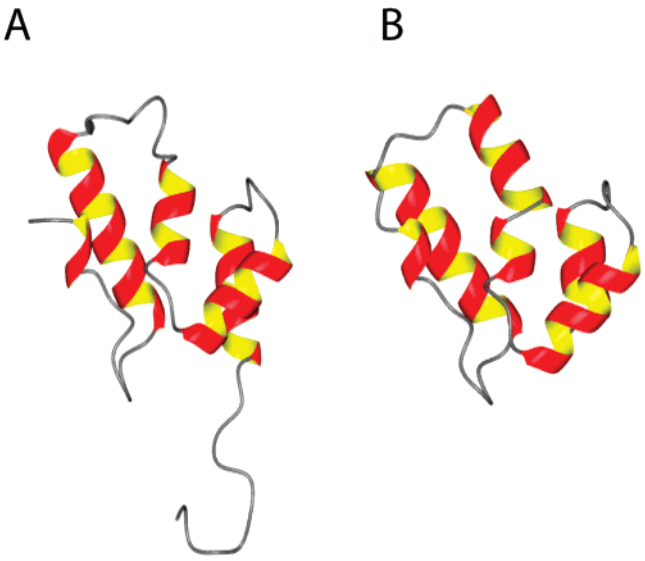

FIGURE 3: Ribbon diagrams generated by MolMol showing: (A) energy-minimized average NMR structure of the double mutant CTD on the left, and (B) the crystal structure of wt CTD from the face-to-face dimer (*6*) on the right. The N-terminus is on the left side in both figures, followed by a short 3_{10} helix and helices 1 to 4. The well-defined kink in helix-2 of the wt CTD crystal structure is clearly visible. The residues near the C-terminus are disordered in the crystal structure. The Supporting Information has a figure of the NMR structure with all the side chains.

in the face-to-face dimer (*7*). The rmsd between these two structures for the backbone Cα atoms for the residues in the four helices chosen for best fit superposition is 1.31 Å, whereas for the superposition of the well-defined backbone Cα atoms of residues 148−219 in the crystal structure it is 3.41 Å. Significant differences between the NMR structure of the double mutant CTD and the wt CTD in the face-to-face dimer are as follows: (i) Helix-2 is shorter in the NMR structure, with a corresponding increase in the loop length between helices 1 and 2. (ii) The kink seen at Thr188 in helix-2 of the wt CTD dimer structure is absent in the NMR structure, where Thr188 appears to be part of a short regular helix composed of residues 186−193. (iii) Helix-4 in the NMR structure is slightly longer. (iv) The packing of the segment of residues 148−158 against helix-1 is also slightly different between the two structures. Figure 5 shows the locations of some residues (181, 184, 185, 189) that were

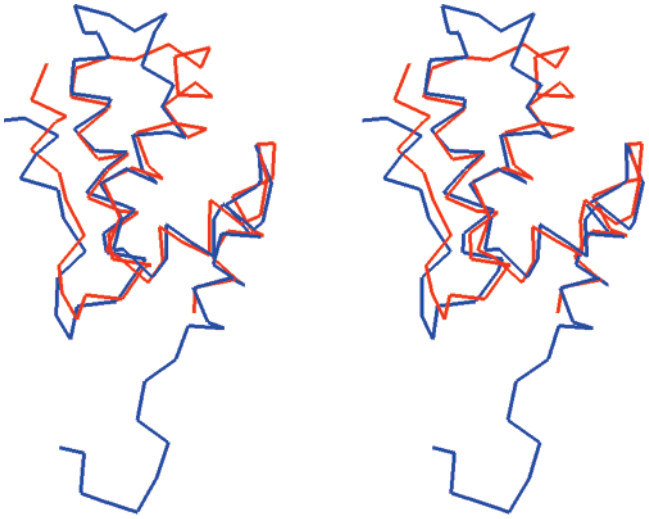

FIGURE 4: Stereoview (cross-eye) of the best-fit superposition of the backbone (Cα atoms) structures of the double mutant CTD (blue) and the wt CTD (red) in the face-to-face dimer. The residues aligned were 160−174 (helix-1), 186−194 (helix-2), 196−205 (helix-3), and 210−221 (helix-4) and resulted in an rmsd of 1.31 Å for these residues. Alignment of all the Cα atoms for residues 148−221 resulted in an rmsd of 3.41 Å.

Table 1: Structural Statistics for the W184A/M185A-CTD NMR Structure

	number of restraints	
NOE distance restraints		
intraresidue	573	
interresidue		
short range	174	
medium range	89	
long range	57	
total NOE restraints	893	
hydrogen bonds (27)[a]	108[a]	
dihedral angle restraints (ϕ, ψ)[b]	76	
residual restraint violations (Å^2)		
CYANA target function	1.09 ± 0.10	
maximum violations:		
upper limits	0.32 ± 0.03	
lower limits	0.05 ± 0.02	
van der waals	0.12 ± 0.01	
torsion angles (deg)	3.72 ± 0.36	
	residues 148−220	helices[c]
average rmsd (Å)		
backbone	1.04	0.35
heavy atom	1.49	0.79
Ramachandran analysis (%)[d]		
residues in most favorable regions		81
residues in additional allowed regions		17
residues in generously allowed regions		2
residues in nonallowed regions		0

[a] A total of 27 hydrogen bonds were included from H/D exchange data, with each defined by two distance constraints (NH−O and N−O). The number 108 refers to the sum of lower and upper bounds for these. [b] Derived from TALOS and from coupling constants measured in HNHA data. [c] Residues 161−172, 185−192, 197−205, and 211−219 were used. [d] Excluding glycine and proline.

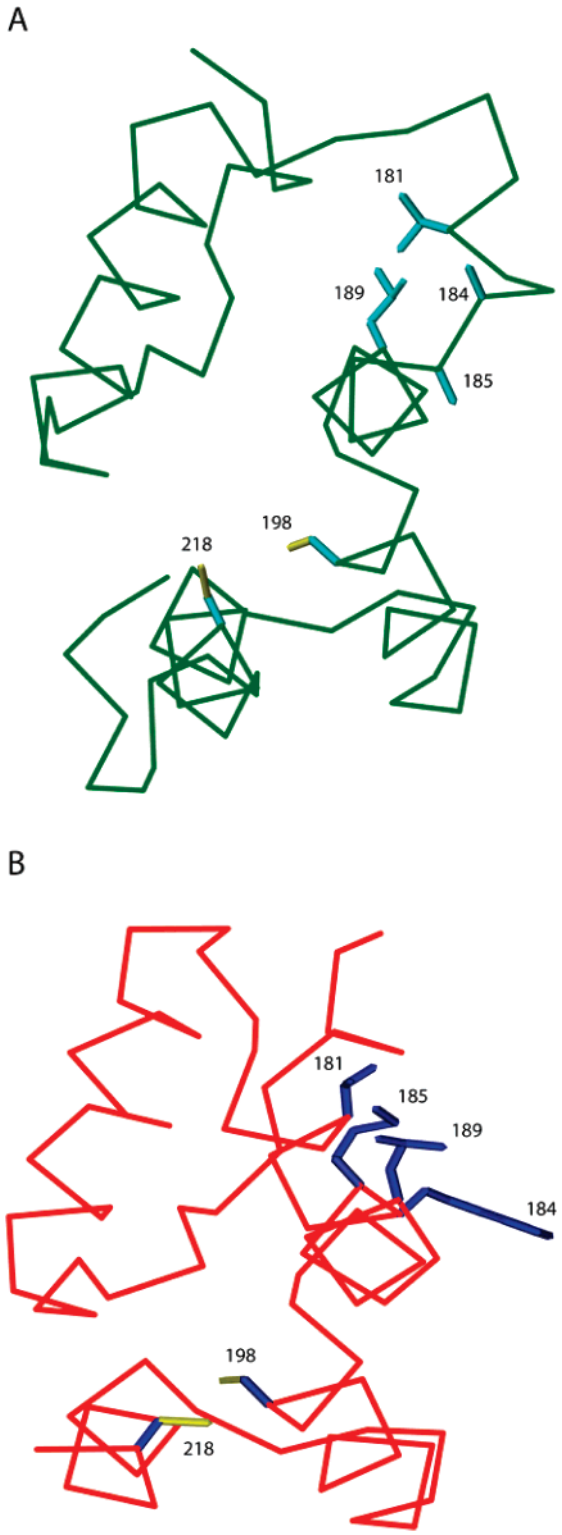

FIGURE 5: Location of some of the key residues (181, 184, 185, and 189) in the NMR structure of the double mutant CTD (A) that were found to be part of the hydrophobic core in the crystal structure of the wt CTD face-to-face dimer (*6*) shown in (B). The view is presented looking through the axis of helix-2, with its carboxy-terminal end toward the viewer. Because of the kink, the top part of the helix-2 in the wt CTD dimer crystal structure deviates from the helix axis of the bottom part. The two reduced cysteines (198 and 218) are also shown.

known to be part of the hydrophobic core in the face-to-face dimer of the wt CTD (*6*) and a comparison of their locations in the double mutant CTD NMR structure. It also shows two reduced cysteines (198 and 218) in the NMR structure. All the peaks in the ^{15}N-HSQC spectrum of the double mutant were successfully assigned by a combination of 3D-NMR experiments on a ^{15}N/^{13}C-labeled protein (see Materials and Methods); the HSQC spectrum with assignments is shown in Figure 6. Some representative sequential connectivities in HNCA and HNCACB spectra are shown in Figure 7 (and additional 3D-NMR spectra are included in the Supporting Information). To determine if the solution conformation of the W184A/M185A-CTD is retained in the wt CTD, the CD spectra of the full-length double mutant CA and the full-length wt CA were recorded. The data are shown in Figure 8 together with an analysis of the secondary structure content in the table. The data show that the conformation of the double mutant CA (and of the CTD) in solution is preserved in the wt CA also with the weak monomer−dimer equilibrium having a negligible effect on the secondary structure content, though some secondary structural elements could differ in their segmental flexibility between the two. To establish that the double mutant protein is monomeric under the concentrations used in the NMR study, we have recorded the HSQC spectra at 0.75 mM and 3 mM (see Supporting Information); the spectra, and in particular the chemical shifts of all the interface residues such as A184 and A185, were virtually identical, indicating that the dimer population is too small to perturb the shifts.

Sticht et al. (*31*) investigated the binding of an inhibitor peptide to the CTD and did a foot-printing of the binding site using the double mutant CTD. The assignments for the peaks visible in the small window of their ^{15}N-HSQC spectrum at 25 °C are in agreement with our assignments at 30 °C (some shifts are due to the temperature difference). While this manuscript was under preparation, Alcaraz et al. (*23*) have reported the NMR structure of the W184A CTD mutant of HIV-1 (pdb file 2JO0). However, their NMR structures differ significantly (rmsd ∼ 12 Å) from our NMR structure as well as from the wt CTD in the face-to-face dimer. An examination of the family of structures in the pdb file 2JO0 shows that helix-2 is essentially missing in about half of the structures while in others it appears as a short three-to-five residue helical turn. Further, that region was found to be highly dynamic in their structure whereas we observe a well-defined eight-residue helix-2 in our structure with sequential connectivities shown in Figure 1 (as well as interhelical NOE contacts involving this helix with other helices, see Supporting Information). Further, helices 3 and 4 in their NMR structure are rotated by nearly 90° with respect to similar helices in the wt CTD structure in the face-to-face dimer, whereas in our study we find them in alignment with the wt CTD helices (Figure 4). The exact origin of these differences between the two NMR structures is not clear. One possible reason could be the differences in the pH where the NMR measurements were performed. Alcaraz et al. performed NMR measurements at pH 7 whereas we used pH 5 to minimize amide hydrogen exchange broadening. It is known that pH has an effect on the shapes of the assembled structures in *in vitro* CA assembly as well as on the hydrodynamic radii of CA dimers (*32*, *33*) which in turn might reflect that the monomer conformations may themselves be slightly sensitive to pH differences. It was also suggested, based on equilibrium denaturation studies, that the monomeric wt CTD has low conformational stability (*34*). Recently, the wt CTD domain

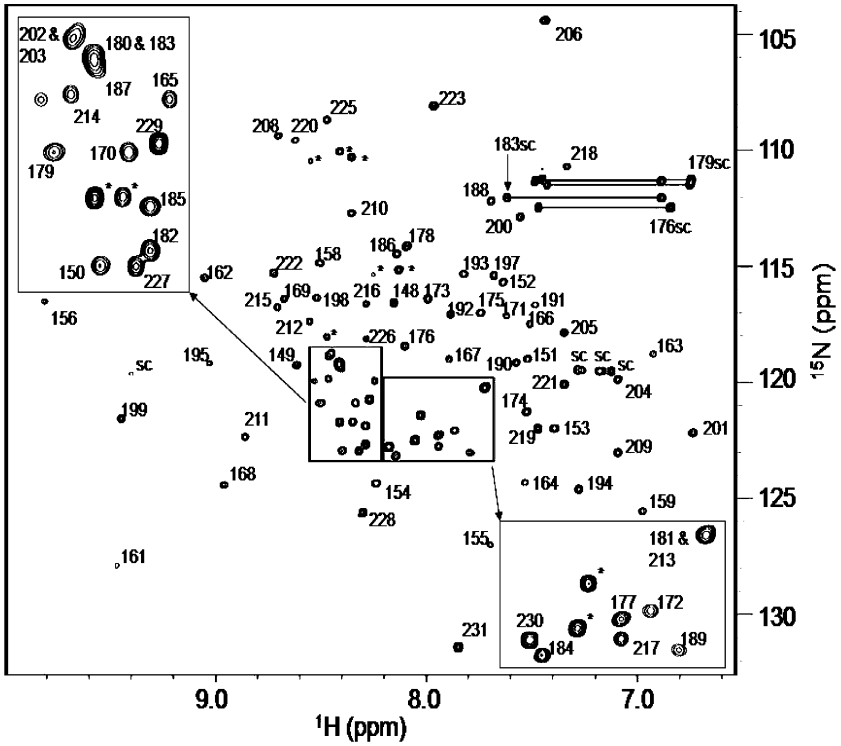

FIGURE 6: ^{15}N-HSQC spectrum of W184A/M185A-CTD with the assignments. sc and * refer to signals from the side chains and the his-tag, respectively.

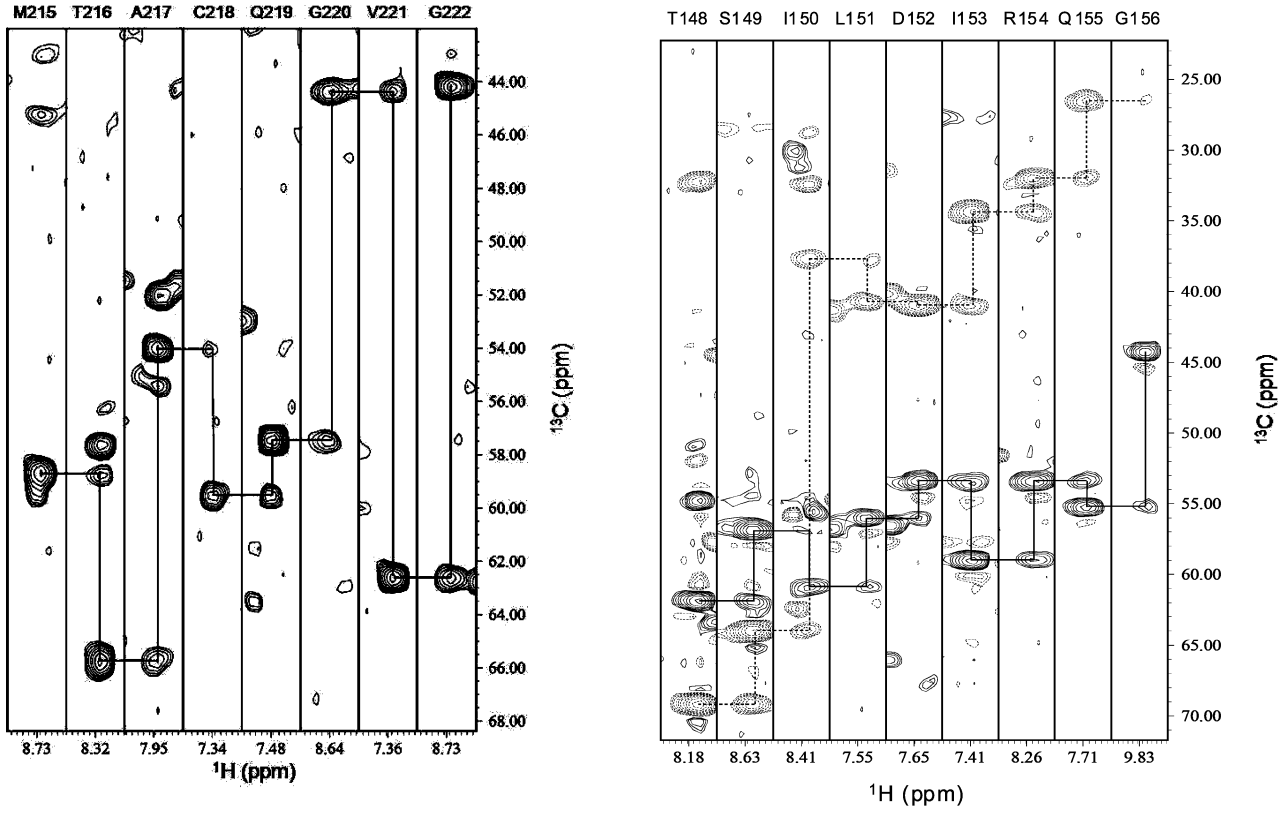

FIGURE 7: Representative panels of (A) HNCA (residues 215−222) and (B) HNCACB (residues 148−156) data showing sequential connectivities. Additional data are in the Supporting Information.

at pH 7 was shown to interact with human lysyl-tRNA synthetase (*35*), and that the interaction involved residues in helix-4 as well as His226 in the disordered region. Thus, it will be interesting to further investigate the pH dependence of the plasticity of the CTD conformation and of the full-length CA using appropriate mutants. It should be noted however that with the exception of His226 (random coil pK_a $\sim$ 7.0) which is located in the disordered C-terminal part of

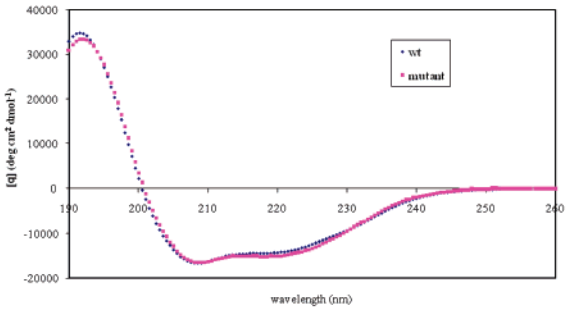

Analysis of CD data in terms of secondary structure content using CD Pro

Protein	helix	strand	turn	unordered
wt	51.2%	11.0%	13.0%	24.8%
mutant	51.5%	10.7%	13.4%	24.0%

FIGURE 8: Far-UV CD spectra for the full-length wild type HIV-1 CA (black) and the W184A/M185A mutant of the full-length CA (purple). The spectra were recorded on an Aviv 400 CD spectrometer in 25 mM sodium phosphate buffer, pH 5 at 20 C. Protein concentration was 7.5 μM. The table shows the analysis of the secondary structural elements using CDPro.

the CTD, all the other His residues of CA are in the NTD domain. The CTD also contains several Glu and Asp residues (random coil pK_a values of 4.3 and 3.9, respectively). Whereas we observed all the expected peaks in the HSQC spectrum at pH 5, Alcaraz et al. (*23*) noted that they could identify only 63 out of the expected 80 peaks in their ^{15}N-HSQC spectrum; these missing peaks are likely to be from the highly disordered regions of the protein where the amide protons can experience significant exchange broadening at the higher pH. The interaction of the wt CTD with the p2 and NC domains was studied by Newman et al. (*36*) using the CA^{CTD}-p2-NC construct. As expected, this construct exhibited a monomer−dimer equilibrium, but the study suggests that the transient coil-to-helix propensity of the p2 may explain the slow proteolysis rate of the CA-p2 junction.

DISCUSSION

Because of the critical role played by the CTD domain as the dimerization module during the assembly of the HIV-1 immature and mature capsids and because of the two equally compelling alternate models, viz., the face-to-face dimer and the domain-swapped dimer, that have been proposed as the functional forms of the CTD dimers, it is important to determine the precise conformation of the CTD domain in its monomeric form to determine if the very process of dimer formation induces dimerization-induced conformational changes. This study is motivated by our desire to determine such a monomeric CTD conformation. Accordingly, we have selected the W184A/M185A mutant of CTD as these two mutations have been shown to significantly shift the monomer−dimer equilibrium toward the predominantly monomeric form without abrogating the assembly activity in the Gag and CA assembly reactions (*9*, *10*, *17*, *18*).

Our NMR study shows that helix-2 (residues 186−193) in the double mutant CTD is much shorter than helix-2 in either the face-to-face dimer (residues 179−193) or the domain-swapped dimer (residues 176−193). This was somewhat unexpected since W184A and M185A mutations were not expected to alter the helix length because of the helical propensity of alanine. Residues 184 and 185 (together with 181) that contributed to hydrophobic interactions (*7*) across the dimeric interface in the crystal structure of the face-to-face dimer are now part of the highly flexible loop joining helices 1 and 2 in the NMR structure (Figure 5). This result suggests that the longer lengths for helix-2 observed in both the crystal structures are probably due to dimerization-induced conformational changes or more precisely due to the presence of a hydrophobic core or a crystalline environment the residues in this helix are exposed to. This observation is further supported by the absence in the NMR structure of the CTD monomer of the well-defined kink at Thr188 seen in the face-to-face dimer (see Figure 3). Our suggestion of dimerization-induced conformational changes in the monomeric units upon complex formation is also in agreement with similar conclusions reached previously based on thermal unfolding studies (*34*). In the NMR structure, Thr188 is part of a well-defined short helix involving residues 186−193 (Figure 3). On the basis of the observation that either a kink or a deviation from ideal helix geometry in helix-2 appears to be present in the monomer structures of other retroviral CA-CTD domains (*19*−*21*), Ivanov et al. (*8*) proposed that a similar kink presumed to exist in the helix-2 of the HIV-1 CTD monomer may provide the driving force to facilitate the dimer swapping under Gag assembly conditions. However, as shown in this work, helix-2 in the double mutant CTD is shorter and the kink is completely absent, suggesting that the kink is likely to be absent in the isolated wt CA (and in wt CTD) as well as in the isolated wt Gag protein if they could be studied at all under monomeric conditions (at extremely low concentrations which is currently beyond the sensitivity capabilities of even a 950 MHz cryoprobe). The CD data in Figure 6 suggests that the secondary structural features of the double mutant CA (and CTD) are maintained in the wt CA in solution, though we cannot rule out differences in segmental flexibility between the two forms.

Even though we utilized DTT throughout during lysis of cells, protein purification, and in the NMR sample tube to keep the two cysteines (Cys198 and Cys218) in a reduced state, in the final energy-minimized structure we note that the two cysteines were spatially close with a S−S distance of 4.2 Å (Figure 5). Similar result was found by Gamble et al. (6) where the wt CTD crystals were grown in the presence of 2 mM mercaptoethanol and yet the two cysteines were within bonding range. We did observe some shifts in some peaks in the HSQC spectra between the oxidized and reduced forms (data not shown) which suggests a further minor change in the relative disposition of helices 3 and 4 (probably moving closer) containing the two cysteines upon oxidation coupled with the exposure of many residues on these two helices to strong ring current fields from the proximal aromatic residues Phe161 and Tyr164 on helix-1. These conformational changes were not investigated further since the reduced form is thought to represent the functional form (*37*).

Implications on Gag and CA Assembly. At this stage, the domain-swapped dimer proposed by Ivanov et al. (*8*, *22*) as an intermediate species during Gag assembly is an intriguing proposal, and further studies may be needed (*38*) to establish the existence of such a dimeric interface playing a role. In

a recent electron cryotomography study of the immature HIV-1 virions, the resolution of the Gag polyproteins in the immature lattice was not adequate enough to differentiate between the face-to-face and domain-swapped CTD dimer models (*1*). If the domain-swapped dimer were indeed shown to play a role in Gag assembly, we propose that the formation of such a dimer is a consequence of and preceded by the formation of an initial *encounter complex* in the form of the face-to-face dimer of two monomeric Gag molecules in which helix-2 from each CA-CTD (i.e., helix-9 in the full-length CA) participates in the hydrophobic dimeric interface and the CTD domains undergo dimerization-induced conformational changes that include the elongation of helix-2 with the development of a kink in the middle that provides the necessary driving force required for domain swapping in the subsequent step, and perhaps aided by additional interactions involving other domains such as the SP1 and NC (*8*). The attractive feature of such a hypothesis is that it combines the best features of both the CTD dimerization models. Thus our NMR study provides a mechanism by which the disparate properties of the face-to-face dimer and the domain-swapped dimer and the results on assembly from mutations in the highly conserved MHR region, and from the mutations on W184 and M185 in the CTD, could all be explained *simultaneously* within the context of Gag assembly. After cleavage of the Gag by the viral protease, the released domain-swapped CA dimer is likely to be metastable and might eventually disassemble (*8*).

While it is not obvious at this stage whether the above proposed mechanism involving a face-to-face dimer as an encounter complex that leads to a domain-swapped dimer formation would be applicable to all the retroviral Gag assemby reactions, we note that the lentiviral CA proteins typically have a Phe/Tyr/Trp in register with W184 and a Leu/Met in register with M185 of HIV-1 CA, suggesting the possibility that these residues may similarly facilitate face-to-face dimerization under assembly reaction conditions, though not necessarily under normal free solution conditions. HIV-1 CA appears to be the only capsid protein that exhibits a weak dimerization with a K_d of $\sim$18 μM, but such a dimerization in solution by itself may be inconsequential to the assembly process.

As mentioned earlier, Ivanov et al. (*8*) have proposed the domain-swapped dimeric interface as an intermediate in Gag assembly. The high-resolution mass spectrometric measurements of amide hydrogen exchange protection factors (*39*) in CA assemblies *in vitro* show that some residues on helix-2 (e.g., W184 and M185) are protected, an observation compatible with a face-to-face dimeric model of the CTD domains. Because of the unavailability of a peptic fragment involving predominantly the MHR domain residues, it was not possible to detect exchange protection in the residues implicated in the dimeric interface of the domain-swapped dimer model (e.g., Y164, Q155). Nevertheless, such a domain-swapped dimer of isolated CA molecules may be unlikely to be participating in *in vitro* CA assembly reactions because of the high-energy barrier to overcome for domain exchange (*8*, *38*). Thus, the *in* vitro CA assembly appears to involve the monomeric wt CA forming face-to-face dimers initially which then leads to other interdomain contacts involving NTD−NTD and NTD−CTD (*39*) as observed in the mature hexameric lattice. The observation of Lanman et al. (*17*) that mutations at W184 significantly slow down the CA assembly rate is consistent with the fact that such mutations shift the monomer−dimer equilibrium to predominantly monomeric conditions. When such a mutant protein forms a dimer under assembly conditions (high salt and pH), the perturbed dimeric interface might be manifesting itself into low fidelity assembly with irregular shaped assembly products (*9*, *10*).

Very recently, Ganser-Pornillos et al. (*40*) have reported the electron cryocrystallographic data on a two-dimensional crystal lattice of the mature flattened spherical capsids formed by the full-length R18L CA mutant of HIV-1 in which they discovered that neither of the previous dimeric crystal structures (*6*−*8*) could be fitted as an "intact dimeric unit" into the cryoEM density map. The best fit they obtained was when the CTD units of the face-to-face dimer (*6*, *7*) were separated and fit as monomeric units into the density map. This resulted in a slightly larger separation between the CTD monomers than in the original face-to-face dimer models (*6*, *7*), and it was speculated that a conformational change might be occurring in the face-to-face CTD dimer during assembly (*40*). Their data also appeared to be incompatible with the presence of a domain-swapped CTD dimer in the hexameric lattice of mature HIV-1 CA (*40*). In the density map of the two-dimensional crystal lattice (*40*), helix-9 of CA (corresponding to helix-2 in the CTD in our notation in this paper) exhibits a kink similar to the one seen in the face-to-face dimer model, presumably reflecting a conformational change induced by the CTD dimerization it self (albeit with a slightly altered dimeric interface than in the original face-to-face dimer models (*6*, *7*)) or by the crystalline environment. In contrast, our NMR structure refers to the free solution condition where the helix-2 of the monomeric double mutant CTD is fully exposed to an aqueous environment.

ACKNOWLEDGMENT

The clone for the W184A/M185A double mutant CTD was kindly provided by Prof. Peter Prevelige, Jr., in the Department of Microbiology. The authors thank Prof. Prevelige for a critical reading of the manuscript and for valuable discussions on HIV-1 assembly. The CD data were obtained on an Aviv 400 spectrometer in the Chemistry Department. The authors thank Drs. Mike Jablonsky and Don Muccio for the access to the CD facility.

SUPPORTING INFORMATION AVAILABLE

NMR data showing the HSQC spectra at two different concentrations, additional representative 3D-NMR data, and the energy-minimized average structure of the W184A/M185A-CTD mutant with side chains. This material is available free of charge via the Internet at http://pubs.acs.org.

REFERENCES

1. Wright, E. R., Schooler, J. B., Ding, H. J., Kieffer, C., Fillmore, C., Sundquist, W. I., and Jensen, G. J. (2007) Electron cryotomography of immature HIV-1 virions reveals the structure of the CA and SP1 Gag shells, *EMBO J. 26*, 2218−2226.
2. Freed, E. O. (1998) HIV-1 Gag proteins: diverse functions in the virus life cycle, *Virology 25*, 1−15.
3. Adamson, C. S., and Jones, I. M. (2004) The molecular basis of HIV capsid assembly − five years of progress, *Rev. Med. Virol. 14*, 107−121.

4. Turner, B. G., and Summers, M. F. (1999) Structural biology of HIV, *J. Mol. Biol. 285*, 1−32.
5. Gitti, R. K., Lee, B. M., Walker, J., Summers, M. F., Yoo, S., and Sundquist, W. I. (1996) Structure of the amino-terminal core domain of the HIV-1 capsid protein, *Science 273*, 231−235.
6. Gamble, T. R., Yoo, S., Vajdos, F. F., von Schwedler, U. K., Worthylake, D. K., Wang, H., McCutcheon, J. P., Sundquist, W. I., and Hill, C. P. (1997) Structure of the carboxyl-terminal dimerization domain of the HIV-1 capsid protein, *Science 278*, 849−853.
7. Worthylake, D. K., Wang, H., Yoo, S., Sundquist, W. I., and Hill, C. P. (1999) Structures of the HIV-1 capsid protein dimerization domain at 2.6 A resolution, *Acta. Crystallogr., Sect. D: Biol. Crystallogr. 55*, 85−92.
8. Ivanov, D., Tsodikov, O. V., Kasanov, J., Ellenberger, T., Wagner, G., and Collins, T. (2007) Domain-swapped dimerization of the HIV-1 capsid C-terminal domain, *Proc. Natl. Acad. Sci. U.S.A. 104*, 4353−4358.
9. Ganser-Pornillos, B. K., von Schwedler, U. K., Stray, K. M., Aiken, C., and Sundquist, W. I. (2004) Assembly properties of the human immunodeficiency virus Type 1 CA protein, *J. Virol. 78*, 2545−2552.
10. von Schwedler, U. K., Stray, K. M., Garrus, J. E., and Sundquist, W. I. (2003) Functional surfaces of the human immunodeficiency virus type 1 capsid protein, *J. Virol. 77*, 5439−5450.
11. Douglas, C. C., Thomas, D., Lanman, J., and Prevelige, P. E. Jr. (2004) Investigation of N-terminal domain charged residues on the assembly and stability of HIV-1 CA, *Biochemistry 43*, 10435−10441.
12. Ehrlich, L. S., Agresta, B. E., and Carter, C. A. (1992) Assembly of recombinant human immunodeficiency virus type 1 capsid protein *in vitro*, *J. Virol. 66*, 4874−4883.
13. Gross, I., Hohenberg, H., and Krausslich, H. G. (1997) *In vitro* assembly properties of purified bacterially expressed capsid proteins of human immunodeficiency virus. *Eur. J. Biochem. 249*, 592−600.
14. Ganser, B. K., Li, S., Klishko, V. Y., Finch, J. T., and Sundquist, W. I. (1999) Assembly and analysis of conical models for the HIV-1 core, *Science 283*, 80−83.
15. Grattinger, M., Hohenberg, H., Thomas, D., Wilk, T., Muller, B., and Krausslich, H. G. (1999) *In vitro* assembly properties of wild-type and cyclophilin-binding defective human immunodeficiency virus capsid proteins in the presence and absence of cyclophilin A, *Virology 257*, 247−260.
16. Li, S., Hill, C. P., Sundquist, W. I., and Finch, J. T. (2000) Image reconstructions of helical assemblies of the HIV-1 CA protein, *Nature 407*, 409−413.
17. Lanman, J., Sexton, J., Sakalian, M., and Prevelige, P. E., Jr. (2002) Kinetic analysis of the role of intersubunit interactions in human immunodeficiency virus type 1 capsid protein assembly *in vitro*, *J. Virol. 76*, 6900−6908.
18. Datta, S. A., Curtis, J. E., Ratcliff, W., Clark, P. K., Crist, R. M., Lebowitz, J., Krueger, S., and Rein, A. (2007) Conformation of the HIV-1 Gag protein in solution, *J. Mol. Biol. 365*, 812−824.
19. Khorasanizadeh, S., Campos-Olivas, R., and Summers, M. F. (1999) Solution structure of the capsid protein from the human T-cell leukemia virus type-I, *J. Mol. Biol. 291*, 491−505.
20. Jin, Z., Jin, L., Peterson, D. L., and Lawson, C. L. (1999) Model for lentivirus capsid core assembly based on crystal dimers of EIAV p26, *J. Mol. Biol. 286*, 83−93.
21. Campos-Olivas, R., Newman, J. L., and Summers, M. F. (2000) Solution structure and dynamics of the Rous sarcoma virus capsid protein and comparison with capsid proteins of other retroviruses, *J. Mol. Biol. 296*, 633−649.
22. Ivanov, D., Stone, J. R., Maki, J. L., Collins, T., and Wagner, G. (2005) Mammalian SCAN domain dimer is a domain-swapped homolog of the HIV capsid C-terminal domain, *Mol. Cell 17*, 137−143.
23. Alcaraz, L. A., del Alamo, M., Barrera, F. N., Mateu, M. G., and Neira, J. L. (2007) Flexibility in HIV-1 assembly subunits: solution structure of the monomeric C-terminal domain of the capsid protein, *Biophys. J. 93*, 1264−1276.
24. Sambrook, J., Fritsch, E. F., and Maniatis, T. (1989) *Molecular Cloning: A Laboratory Manual*, 2nd ed., Vol. 3, p A.3. Cold Spring Harbor Laboratory Press, Woodbury, NY.
25. Delaglio, F., Grzesiek, S., Vuister, G. W., Zhu, G., Pfeifer, J., and Bax, A. (1995) NMRPipe: a multidimensional spectral processing system based on UNIX pipes, *J. Biomol. NMR 6*, 277−293.
26. Xia, T. H., Bartels, C., and Wüthrich, K. (1993) *XEASY, ETH automated spectroscopy for X-window system, user manual*, ETH-Honggerberg, Zurich.
27. Molday, R. S., Englander, S. W., and Kallen, R. G. (1972) Primary structure effects on peptide group hydrogen exchange, *Biochemistry 11*, 150−158.
28. Bai, Y., Milne, J. S., Mayne, L., and Englander, S. W. (1993) Primary structure effects on peptide group hydrogen exchange. *Proteins 17*, 75−86.
29. Krishna, N. R., Huang, D. H., Chen, D. M., and Goldstein, G. (1980) Solution conformation of thymopoietin$_{32-36}$: a proton nuclear magnetic resonance study, *Biochemistry 19*, 5557−5563.
30. van Gunsteren, W. F., Billeter, S. R., Eising, A. A., Hunenberger, P. H., Kruger, P., Mark, A. E., Scott, W. R. P., and Tironi, I. G. (1996) *Biomolecular Simulation: The GROMOS96 Manual and User Guide*, VdF: Hochschulverlag AG an der ETH Zurich and BIOMOS b.v, Zurich, Gronigen.
31. Sticht, J., Humbert, M., Findlow, S., Bodem, J., Muller, B., Dietrich, U., Werner, J., and Krausslich, H. G. (2005) A peptide inhibitor of HIV-1 assembly *in vitro*, *Nature Struct. Mol. Biol. 12*, 671−677.
32. Gross, I., Hohenberg, H., Wilk, T., Wiegers, K., Grättinger, M., Müller, B., Fuller, S., and Kräusslich, H. G. (2000) A conformational switch controlling HIV-1 morphogenesis, *EMBO J. 19*, 103−113.
33. Ehrlich, L. S., Liu, T., Scarlata, S., Chu, B., and Carter, C. A. (2001) HIV-1 capsid protein forms spherical (immature-like) and tubular (mature-like) particles *in vitro*: structure switching by pH-induced conformational changes. *Biophys. J. 81*, 586−594.
34. Mateu, M. G. (2002) Conformational stability of dimeric and monomeric forms of the C-terminal domain of human immunodeficiency virus-1 capsid protein, *J. Mol. Biol. 318*, 519−531.
35. Kovaleski, B. J., Kennedy, R., Khorchid, A., Kleiman, L., Matsuo, H., and Musier-Forsyth, K. (2007) Critical role of helix 4 of HIV-1 capsid c-terminal domain in interactions with human lysyl-tRNA synthetase. *J. Biol. Chem. 282*, 32274−32279.
36. Newman, J. L., Butcher, E. W., Patel, D. T., Mikhaylenko, Y., and Summers, M. F. (2004) Flexibility in the P2 domain of the HIV-1 Gag polyprotein. *Protein Sci. 13*, 2101−2107.
37. Homme, M. B., Carter, C., and Scarlata, S. (2005) The Cysteine Residues of HIV-1 Capsid Regulate Oligomerization and Cyclophilin A-induced Changes, *Biophy. J. 88*, 2078−2088.
38. Kingston, R. L., and Vogt, V. M. (2005) Domain swapping and retroviral assembly, *Mol. Cell 17*, 166−167.
39. Lanman, J., Lam, T. T., Barnes, S., Sakalian, M., Emmett, M. R., Marshall, A. G., and Prevelige, P. E., Jr. (2003) Identification of novel interactions in HIV-1 capsid protein assembly by high-resolution mass spectrometry, *J. Mol. Biol. 325*, 759−772.
40. Ganser-Pornillos, B. K., Cheng, A., and Yeager, M. (2007) Structure of full-length HIV-1 CA: a model for the mature capsid lattice, *Cell 131*, 70−79.

BI7022128